Supporting Information for:

Self-assembled colloidal gold superparticles to enhance the sensitivity of lateral flow immunoassays with sandwich format

Xirui Chen[a,b‡], Yuankui Leng[a,b‡], Liangwen Hao[a,b], Hong Duan[a,b], Jing Yuan[a,b], Wenjing Zhang[a,b], Xiaolin Huang*[a,b], and Yonghua Xiong*[a,b,c]

[a] State Key Laboratory of Food Science and Technology, Nanchang University, Nanchang 330047, P. R. China;

[b] School of Food Science and Technology, Nanchang University, Nanchang 330047, P. R. China;

[c] Jiangxi-OAI Joint Research Institute, Nanchang University, Nanchang 330047, P. R. China;

[‡]These authors contributed equally to this work.

*Correspondence to:

Dr. Xiaolin Huang and Dr. Yonghua Xiong
State Key Laboratory of Food Science and Technology, and Jiangxi-OAI Joint Research Institute, Nanchang University
Address: 235 Nanjing East Road, Nanchang 330047, P.R. China
Phone: +0086-791-8833-4578. Fax: +0086-791-8833-3708
E-mail: hxl19880503@163.com (X. H.); yhxiongchen@163.com (Y. X.)

List of content

Supplementary results

Optimization of the GSP-LFIA and AuNP-LFIA for HCG detection

Several key factors, including the pH value (**Figures S4**), EDC concentration for covalent conjugation of antibody (**Figure S5A to S13A**), and saturated labeling amount of anti-HCG-β mAbs (**Figure S5B to S13B**), that affect the conjugation efficiency of antibody were systematically studied and optimized to obtain the best GSP or AuNP probes. Then, the concentration of anti-HCG-α mAbs sprayed on the T line (**Figure S15**), the GSP or AuNP probe amount used in each strip (**Figures S5C to S13C**), and the running strip time for signal readout (**Figures S5D to S13D**) were studied. The details for the optimal condition combinations that can enable the maximum OD_T in the GSP-LFIA and AuNP-LFIA strips are summarized in **Table S2**.

Optimization of the GSP-LFIA and AuNP-LFIA for HBsAg detection

To obtain the best detection sensitivity, various parameters that influence the sensitivity of $AuNP_{40}$-LFIA and GSP_{270}-LFIA strip, including saturated labeling amount of anti-HBsAg mAb (**Figures S19A** and **S20A**), concentration of anti-HBsAg pAb sprayed on the T line (**Figures S18B** and **S19B**), GSP_{270} or $AuNP_{40}$ probe amount used in each strip (**Figures S19C** and **S20C**), and running strip time for signal readout (**Figures S18D** and **S20D**), were systematically investigated. The results show that the optimal combinations are as follows: saturated labeling amount of anti-HBsAg mAb of 0.38 mg/mL and 10.96 mg/mL, anti-HBsAg pAb of 3.0 mg/mL and 2.5 mg/mL, amount of $AuNP_{40}$ or GSP_{270} probes in each strip of 5.325 fmol and 0.14 fmol for $AuNP_{40}$-LFIA and GSP_{270}-LFIA, respectively.

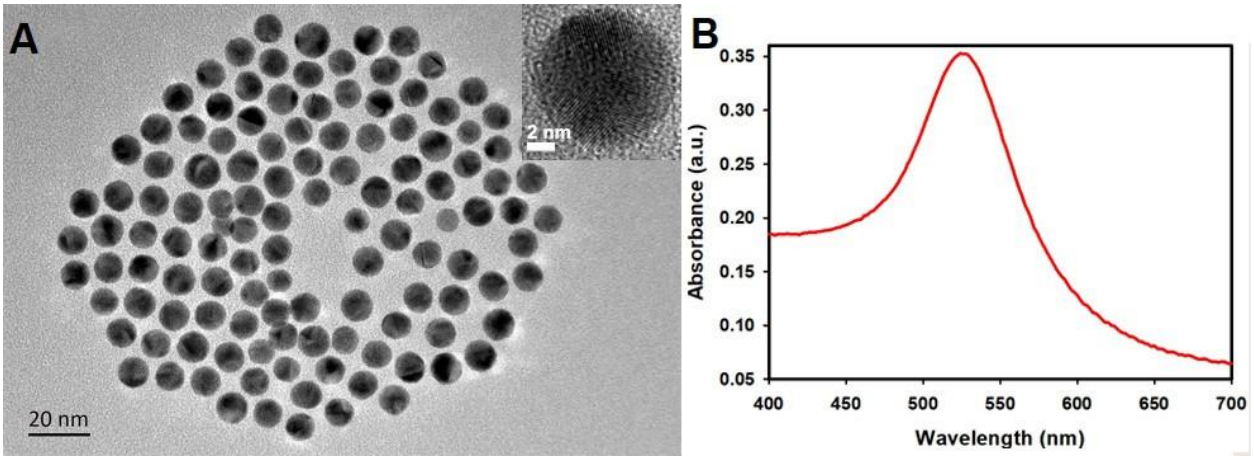

Figure S1. Characterization of oleylamine-coated AuNPs. (A) TEM image. (B) UV–vis absorption spectra. The maximum absorption peak of the hydrophobic AuNPs was located at 524 nm.

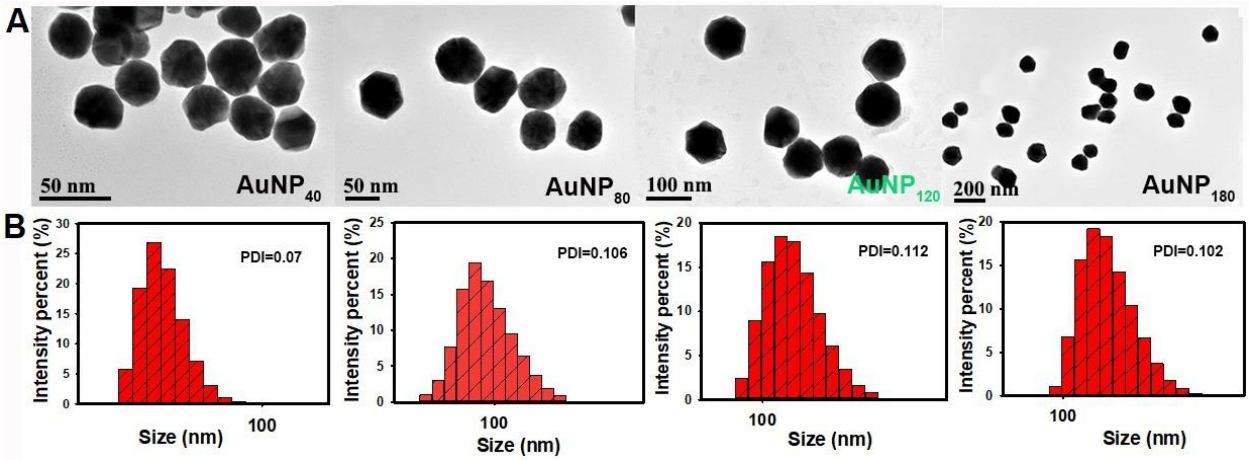

Figure S2. Characterization of different sized-AuNPs. (A) TEM images. (B) DLS analysis. For Figure S2A and S2B, from left to right: $AuNP_{40}$, $AuNP_{80}$, $AuNP_{120}$, and $AuNP_{180,}$ respectively.

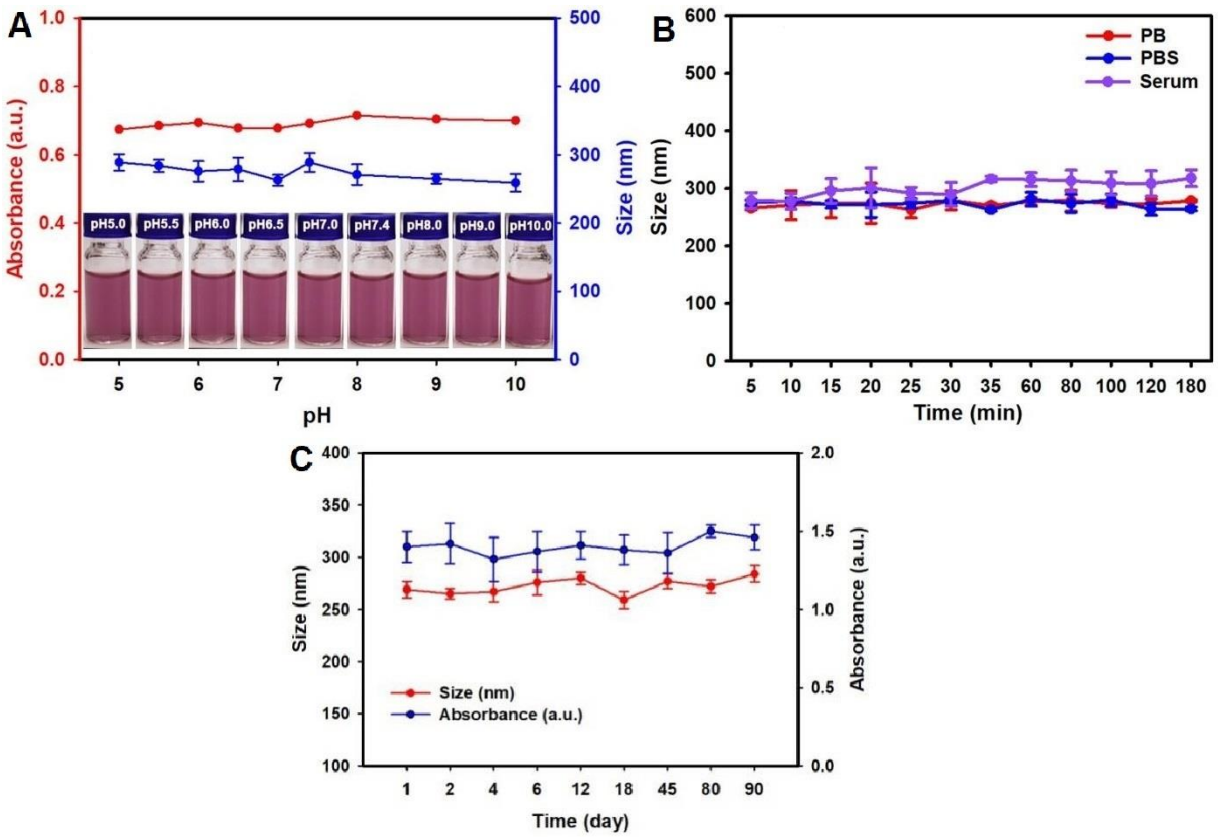

Figure S3. (A) Absorbance and hydrodynamic diameter of GSP_{270} solutions under diverse pH values. The inset reveals the photograph of GSP_{270} solutions under different pH values. (B) Hydrodynamic diameter variations of GSP_{270} dispersed in PB, PBS, and serum against incubation time. (C) Evaluation of the long-term storage stability of GSPs by recording the changes in hydrodynamic diameter and absorbance of GSPs against 90-day storage.

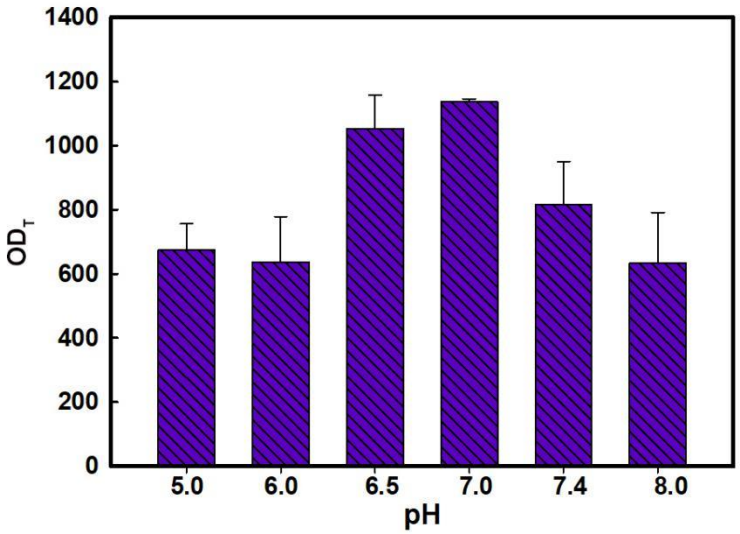

Figure S4. Effect of pH for the conjugation of anti-HCG-β mAb to GSPs or AuNPs.

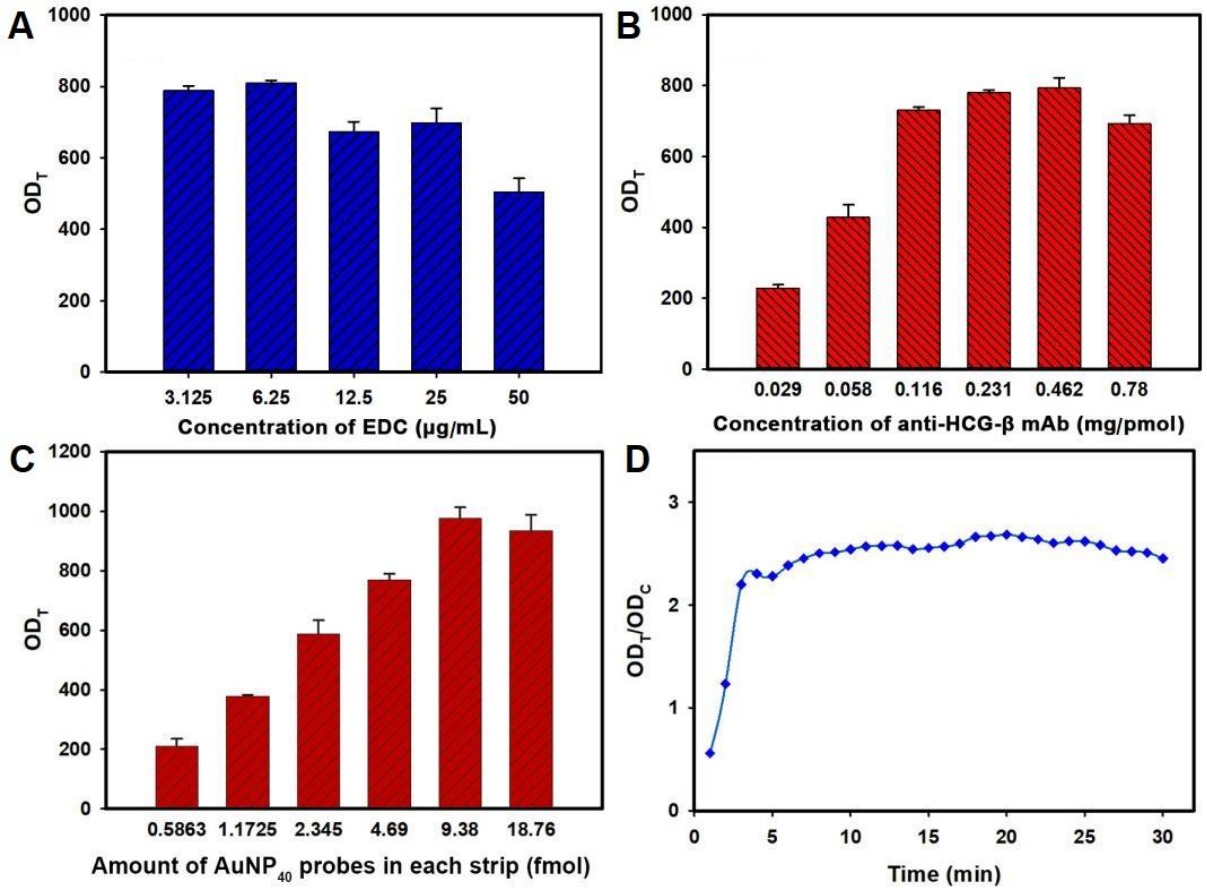

Figure S5. Parameter optimization of $AuNP_{40}$-LFIA for HCG detection. (A) The EDC concentration for the anti-HCG-β mAb conjugation. (B) The saturated labeling amount of anti-HCG-β mAb on the $AuNP_{40}$ surface. (C) The used amount of $AuNP_{40}$ probe in each strip. (D) The optimal readout time after running the strip with the sample solution.

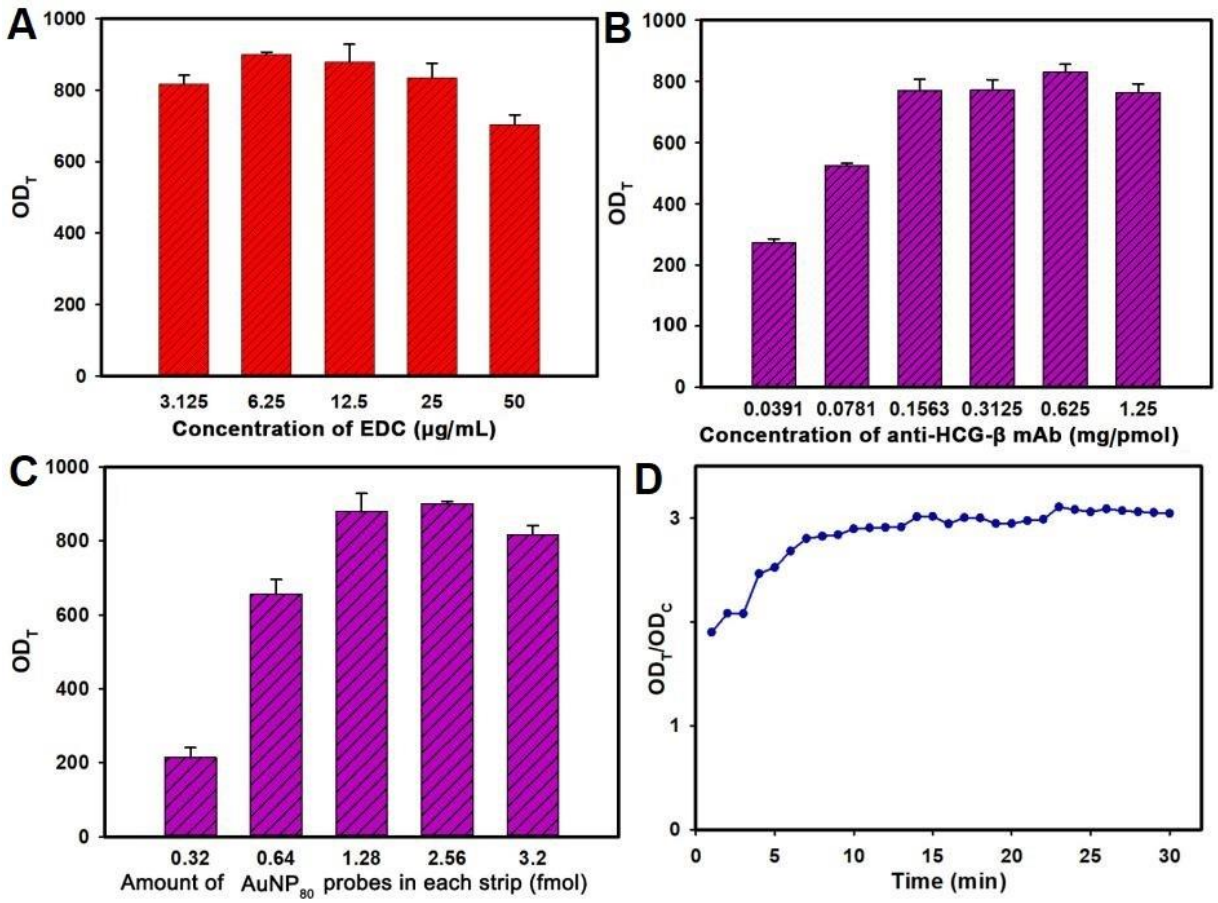

Figure S6. Parameter optimization of $AuNP_{80}$-LFIA for HCG detection. (A) The EDC concentration for the anti-HCG-β mAb conjugation. (B) The saturated labeling amount of anti-HCG-β mAb on the $AuNP_{80}$ surface. (C) The used amount of $AuNP_{80}$ probe in each strip. (D) The optimal readout time after running the strip with the sample solution.

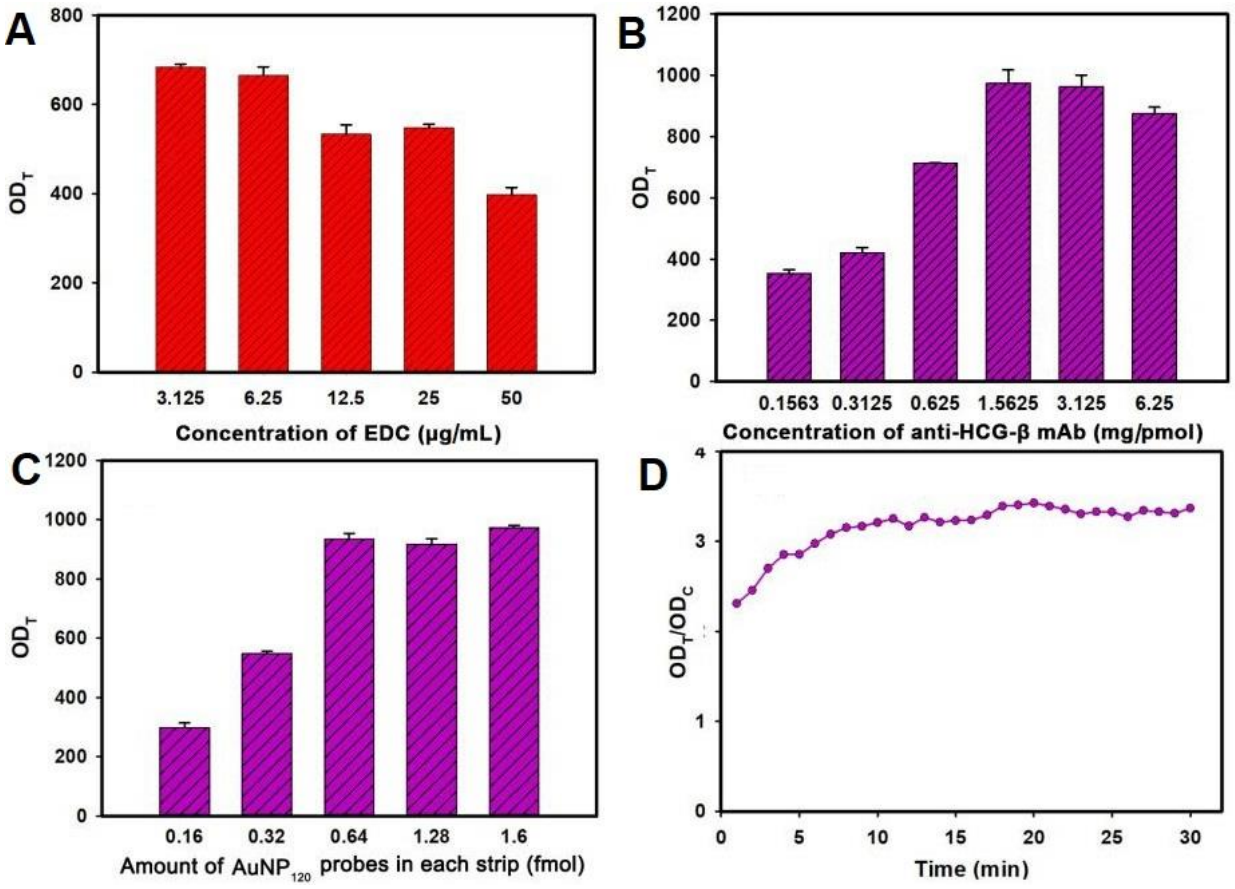

Figure S7. Parameter optimization of $AuNP_{120}$-LFIA for HCG detection. (A) The EDC concentration for the anti-HCG-β mAb conjugation. (B) The saturated labeling amount of anti-HCG-β mAb on the $AuNP_{120}$ surface. (C) The used amount of $AuNP_{120}$ probe in each strip. (D) The optimal readout time after running the strip with the sample solution.

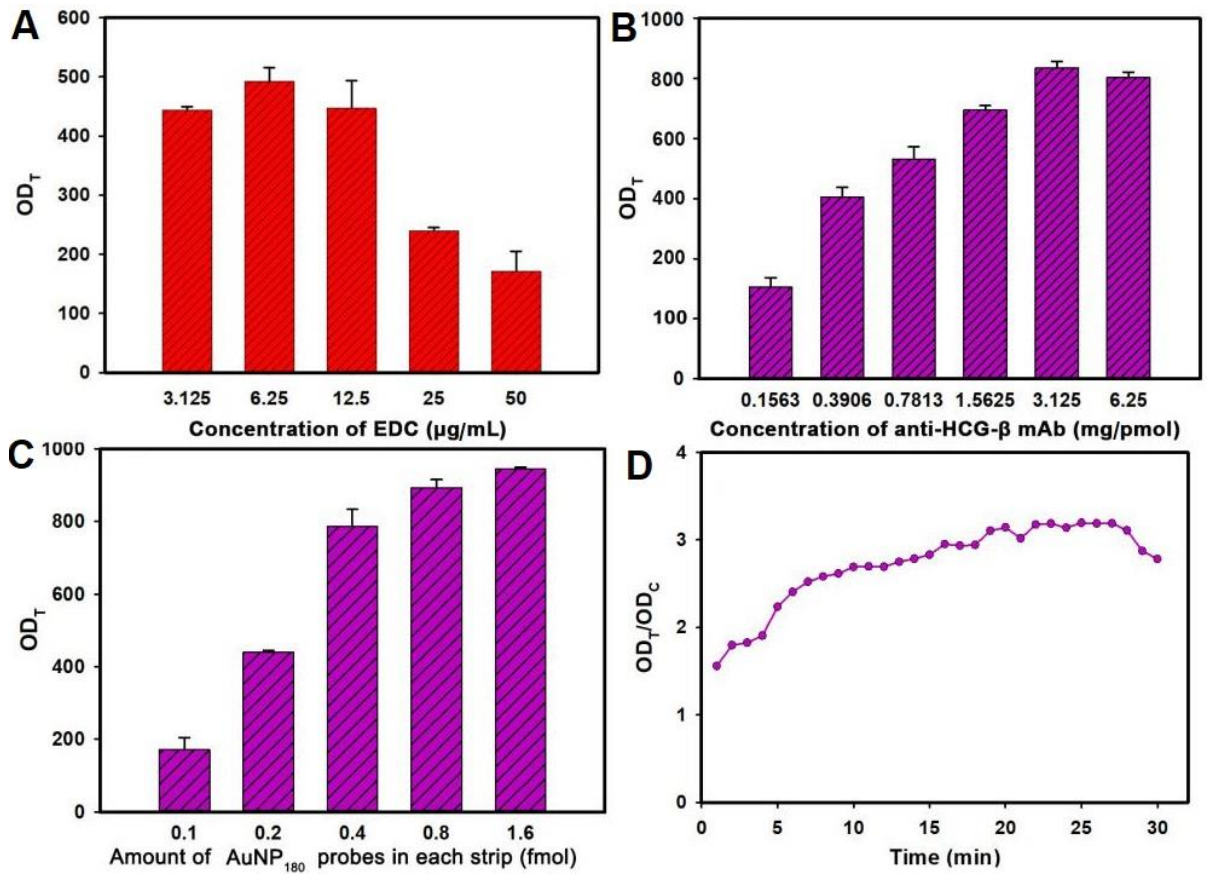

Figure S8. Parameter optimization of $AuNP_{180}$-LFIA for HCG detection. (A) The EDC concentration for the anti-HCG-β mAb conjugation. (B) The saturated labeling amount of anti-HCG-β mAb on the $AuNP_{180}$ surface. (C) The used amount of AuNP180 probe in each strip. (D) The optimal readout time after running the strip with the sample solution.

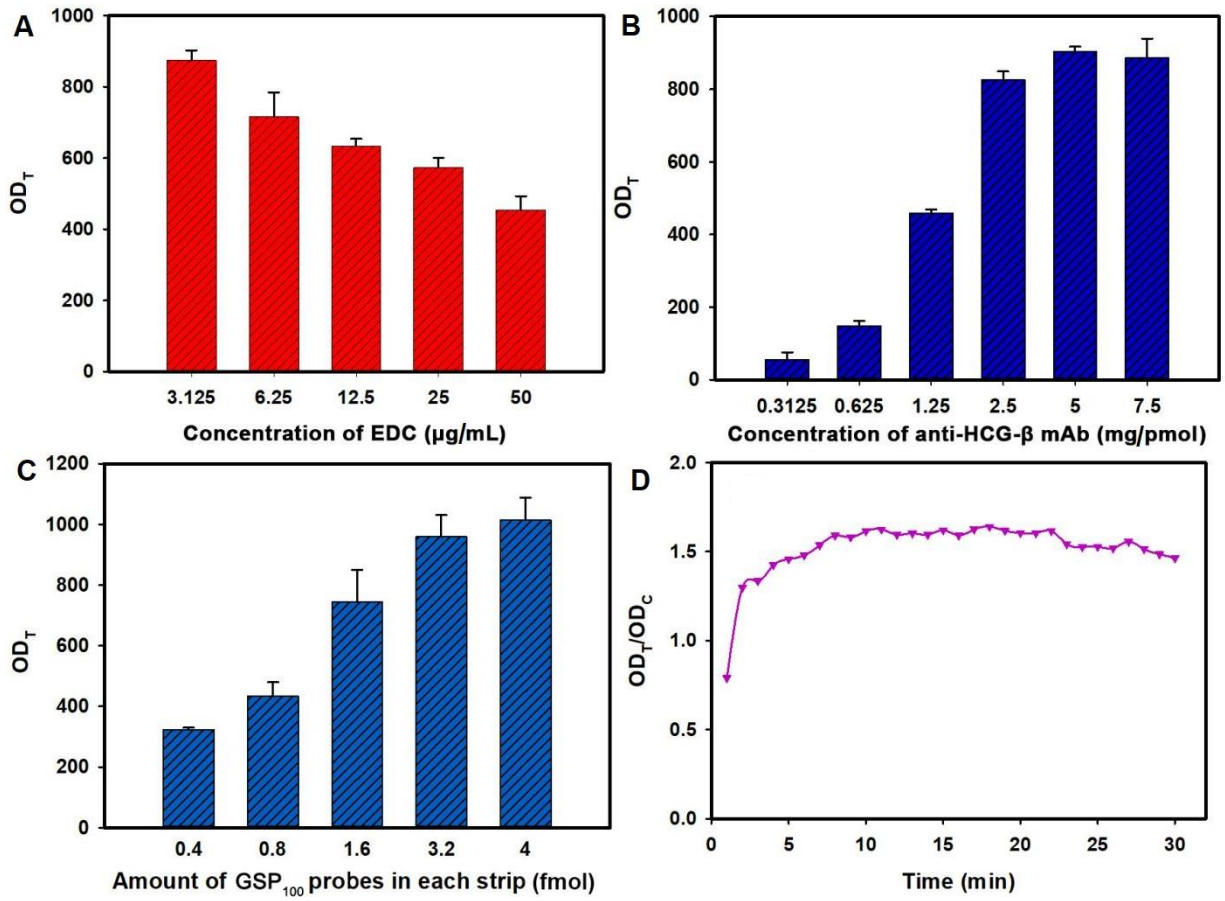

Figure S9. Parameter optimization of GSP_{100}-LFIA for HCG detection. (A) The EDC concentration for the anti-HCG-β mAb conjugation. (B) The saturated labeling amount of anti-HCG-β mAb on the GSP_{100} surface. (C) The used amount of GSP_{100} probe in each strip. (D) The optimal readout time after running the strip with the sample solution.

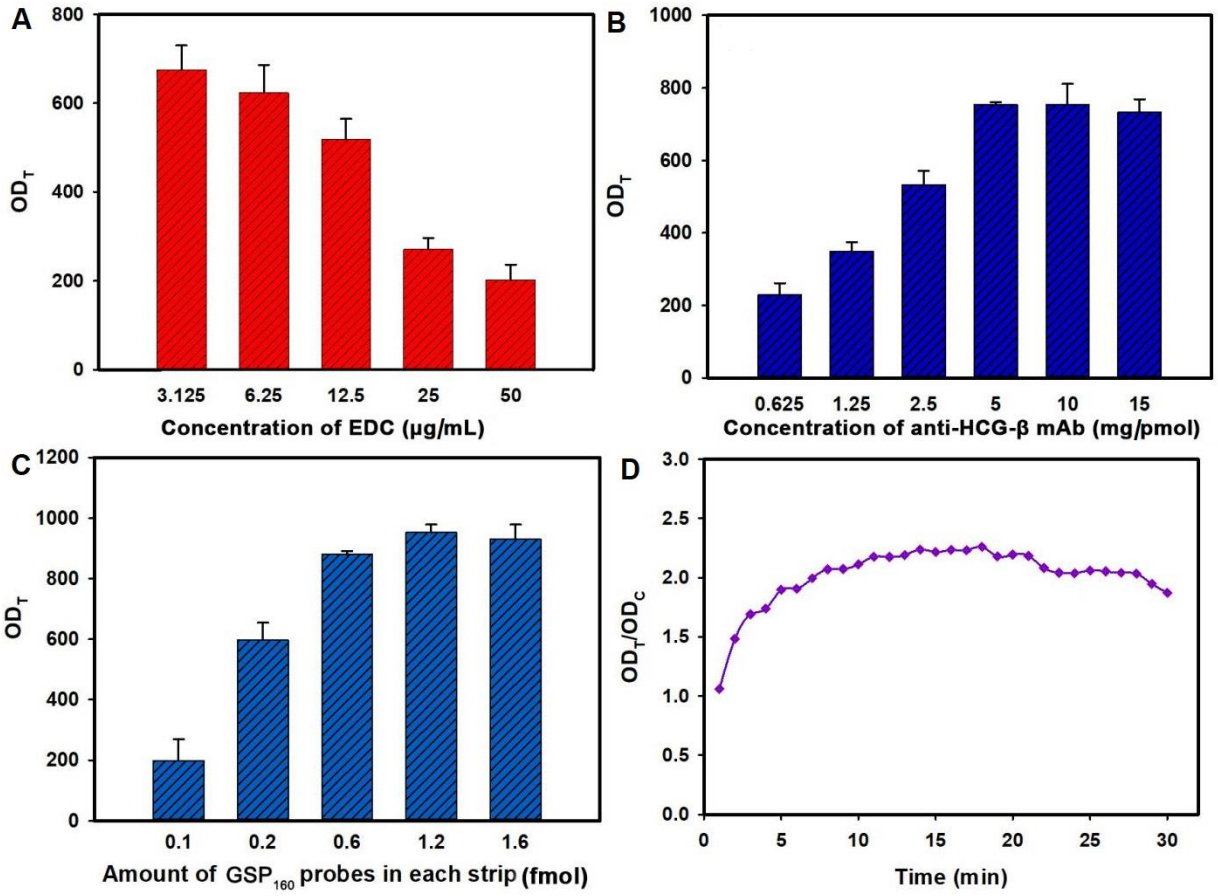

Figure S10. Parameter optimization of GSP_{160}-LFIA for HCG detection. (A) The EDC concentration for the anti-HCG-β mAb conjugation. (B) The saturated labeling amount of anti-HCG-β mAb on the GSP_{160} surface. (C) The used amount of GSP_{160} probe in each strip. (D) The optimal readout time after running the strip with the sample solution.

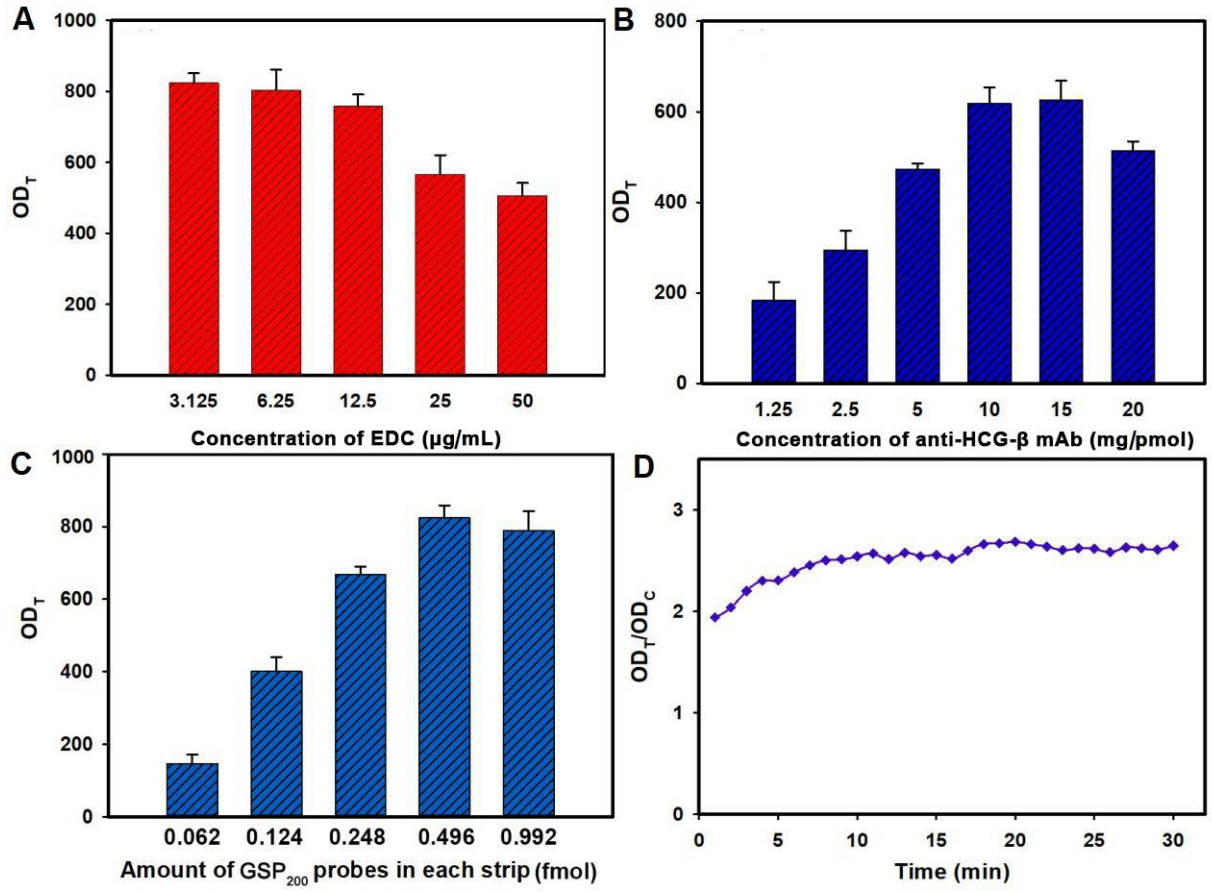

Figure S11. Parameter optimization of GSP_{200}-LFIA for HCG detection. (A) The EDC concentration for the anti-HCG-β mAb conjugation. (B) The saturated labeling amount of anti-HCG-β mAb on the GSP_{200} surface. (C) The used amount of GSP_{200} probe in each strip. (D) The optimal readout time after running the strip with the sample solution.

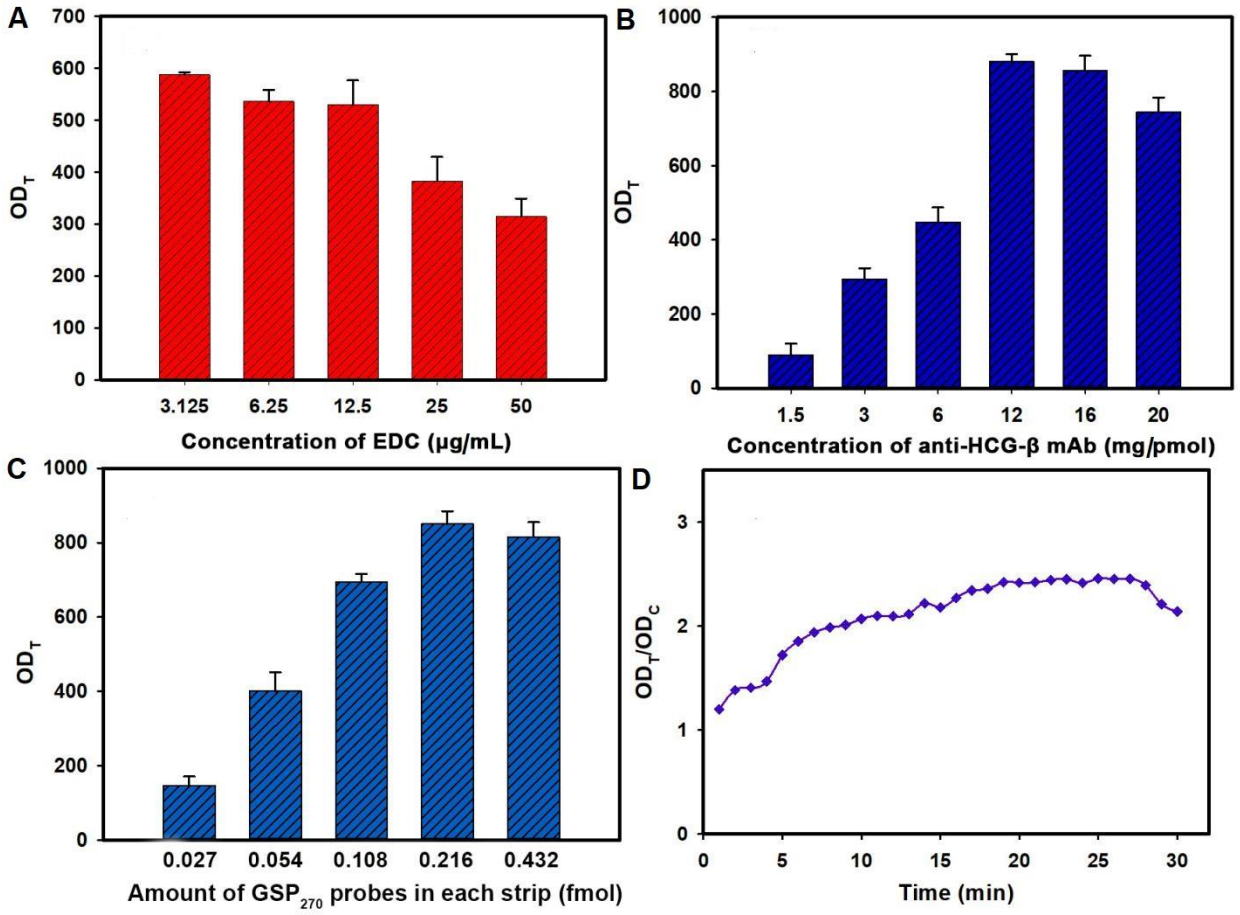

Figure S12. Parameter optimization of GSP_{270}-LFIA for HCG detection. (A) The EDC concentration for the anti-HCG-β mAb conjugation. (B) The saturated labeling amount of anti-HCG-β mAb on the GSP_{270} surface. (C) The used amount of GSP_{270} probe in each strip. (D) The optimal readout time after running the strip with the sample solution.

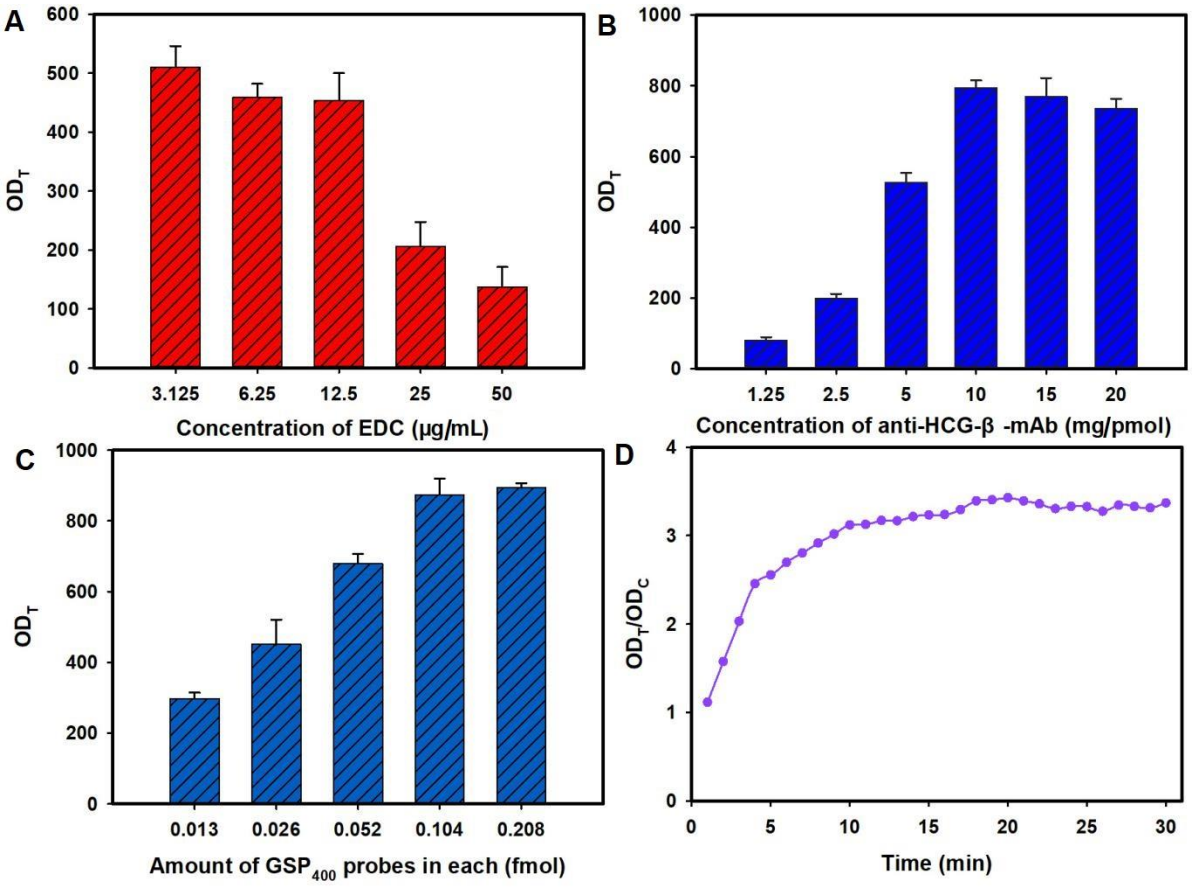

Figure S13. Parameter optimization of GSP_{400}-LFIA for HCG detection. (A) The EDC concentration for the anti-HCG-β mAb conjugation. (B) The saturated labeling amount of anti-HCG-β mAb on the GSP_{400} surface. (C) The used amount of GSP_{400} probe in each strip. (D) The optimal readout time after running the strip with the sample solution.

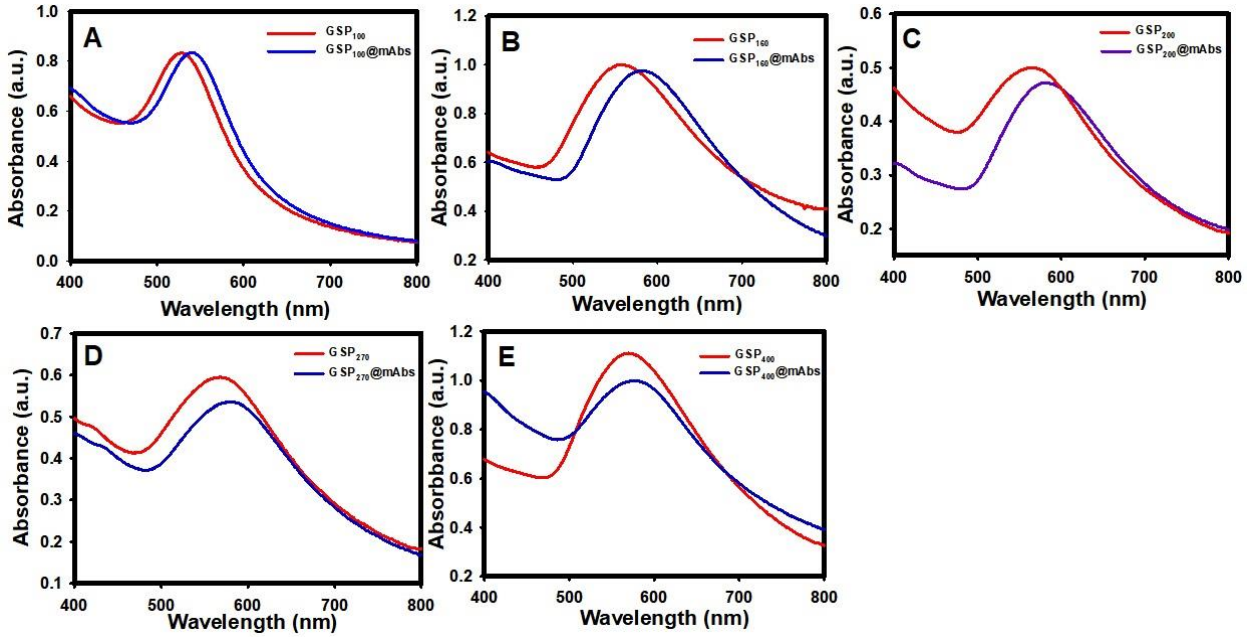

Figure S14. UV-vis absorption spectra for confirming the successful conjugation of GSPs with anti-HCG-α mAb. (A) GSP_{100}, (B) GSP_{160}, (C) GSP_{200}, (D) GSP_{270}, and (E) GSP_{400}.

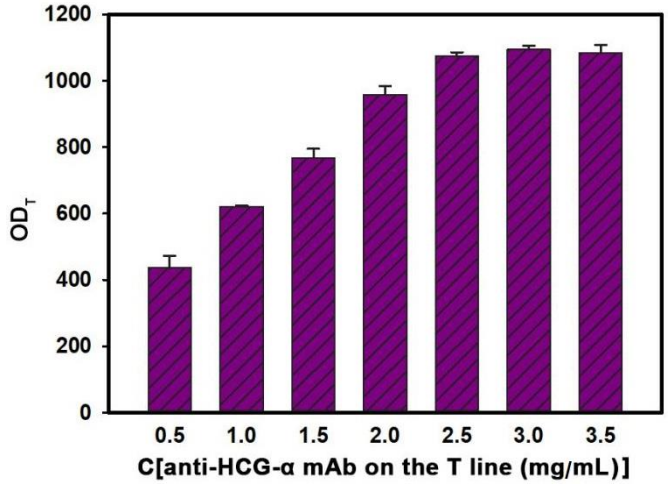

Figure S15. The concentration optimization of anti-HCG-α mAb sprayed on the T line of strip.

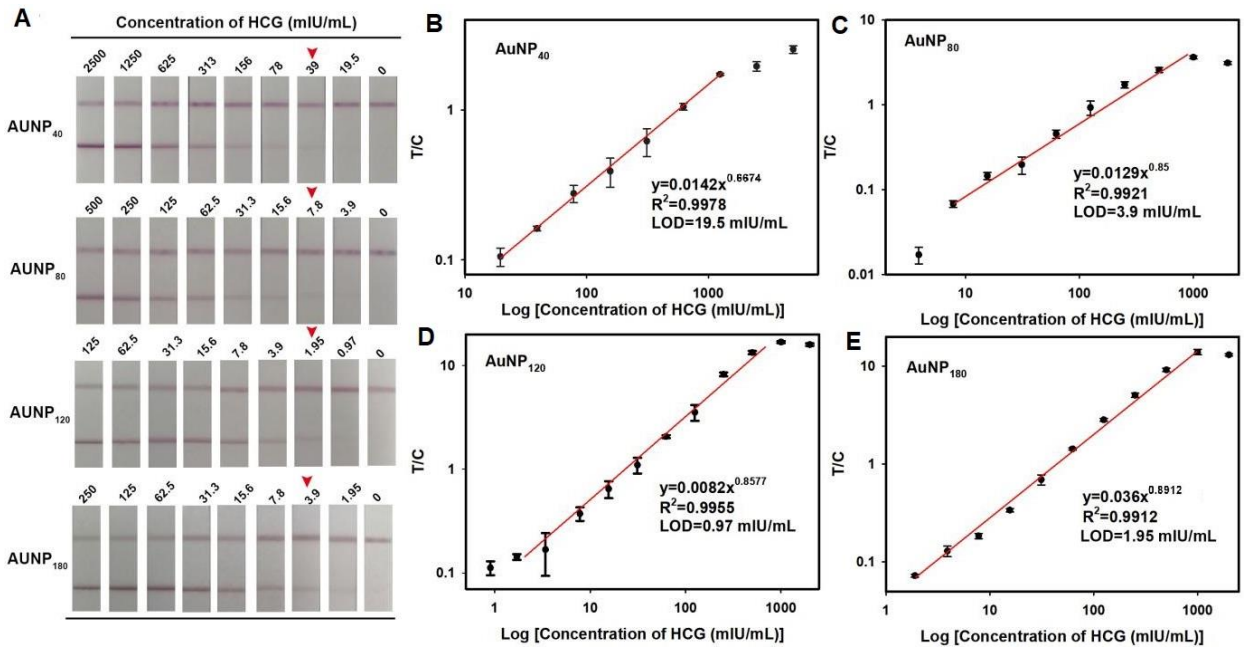

Figure S16. Qualitative and quantitative assay for HCG in serum using AuNP-LFIA. (A) The prototypes of four AuNP-LFIA strips responding to varying HCG concentrations. (B-E) Linear dependences against HCG concentrations of four AuNP-LFIA strips.

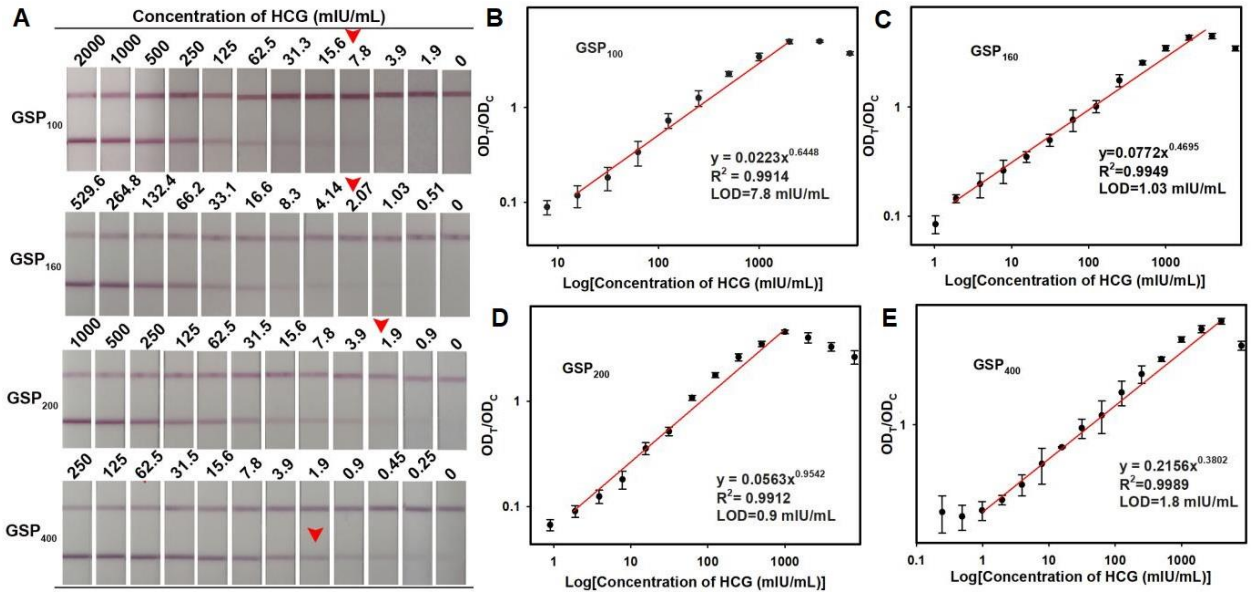

Figure S17. Qualitative and quantitative assay for HCG in serum using GSP-LFIA. (A) The prototypes of four GSP-LFIA strips responding to varying HCG concentrations. (B-E) Linear dependences against HCG concentrations of four GSP-LFIA strips.

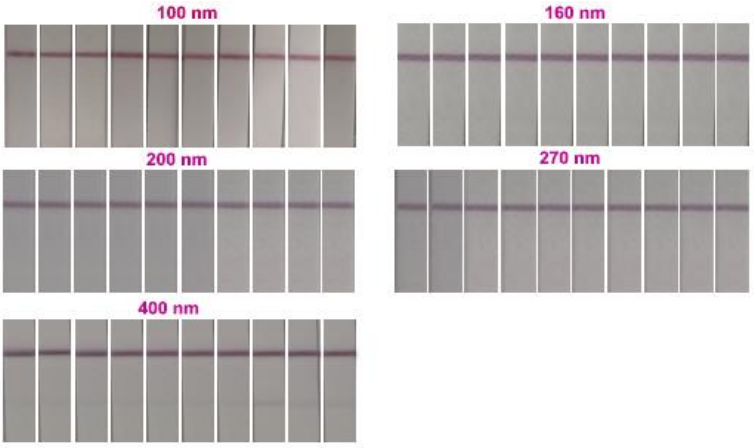

Figure S18. The strip prototypes from the detection of ten HCG-negative serum samples using five different GSP-LFIA strips, respectively. From these pictures, we can see that obvious background bands at the T zones when we used the GSP_{400}-LFIA strip to detect ten blank samples, whereas no background signal was seen with other four GSP-LFIA strips, confirming the fact that 400 nm partly settled in the test area of NC membrane to form background value even in the absence of targets.

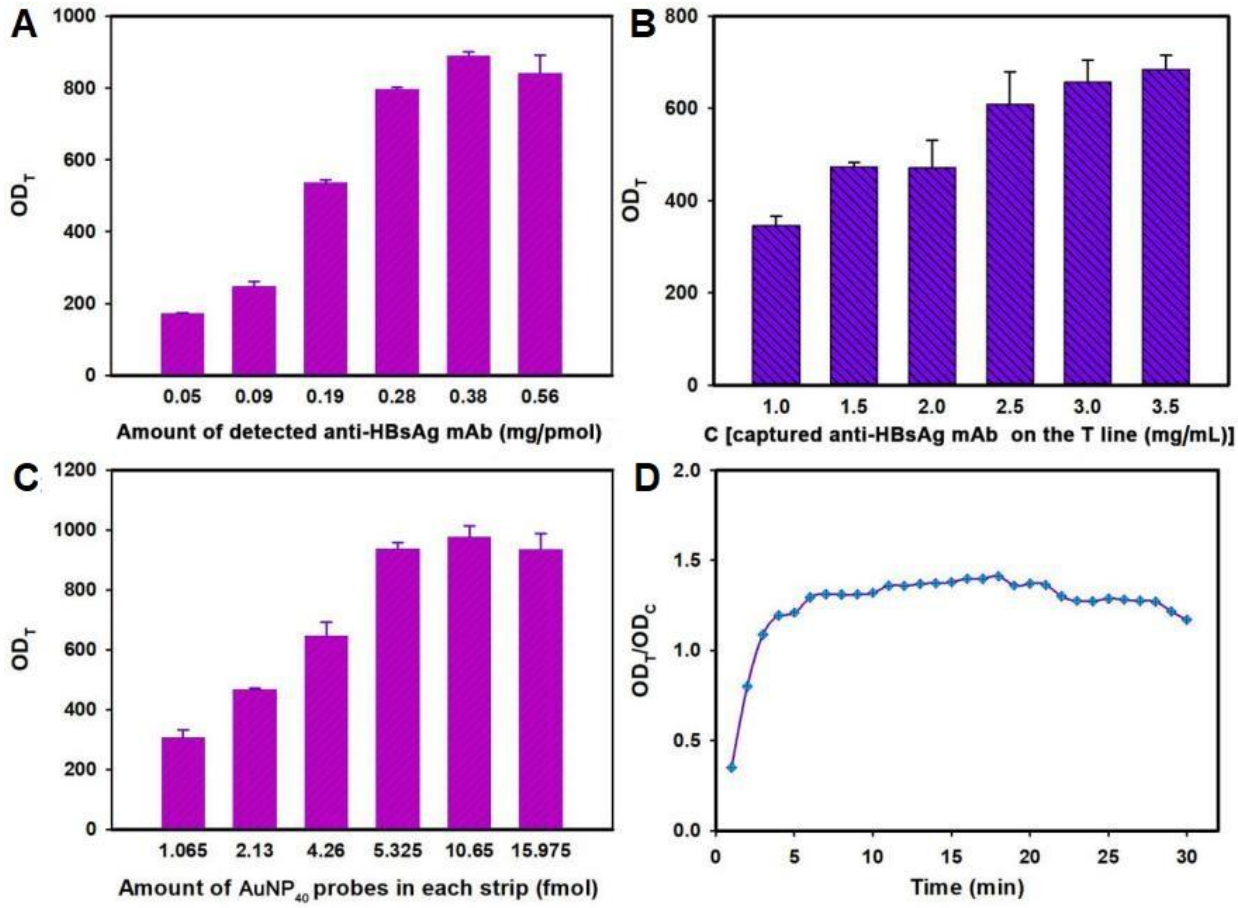

Figure S19. Parameter optimization of $AuNP_{40}$-LFIA for HBsAg detection. (A) The saturated labeling amount of detected anti-HBsAg mAb on the $AuNP_{40}$ surface. (B) The concentration of captured anti-HBsAg mAb sprayed on the T line. (C) The used amount of $AuNP_{40}$ probe in each strip. (D) The optimal readout time after running the strip with the sample solution.

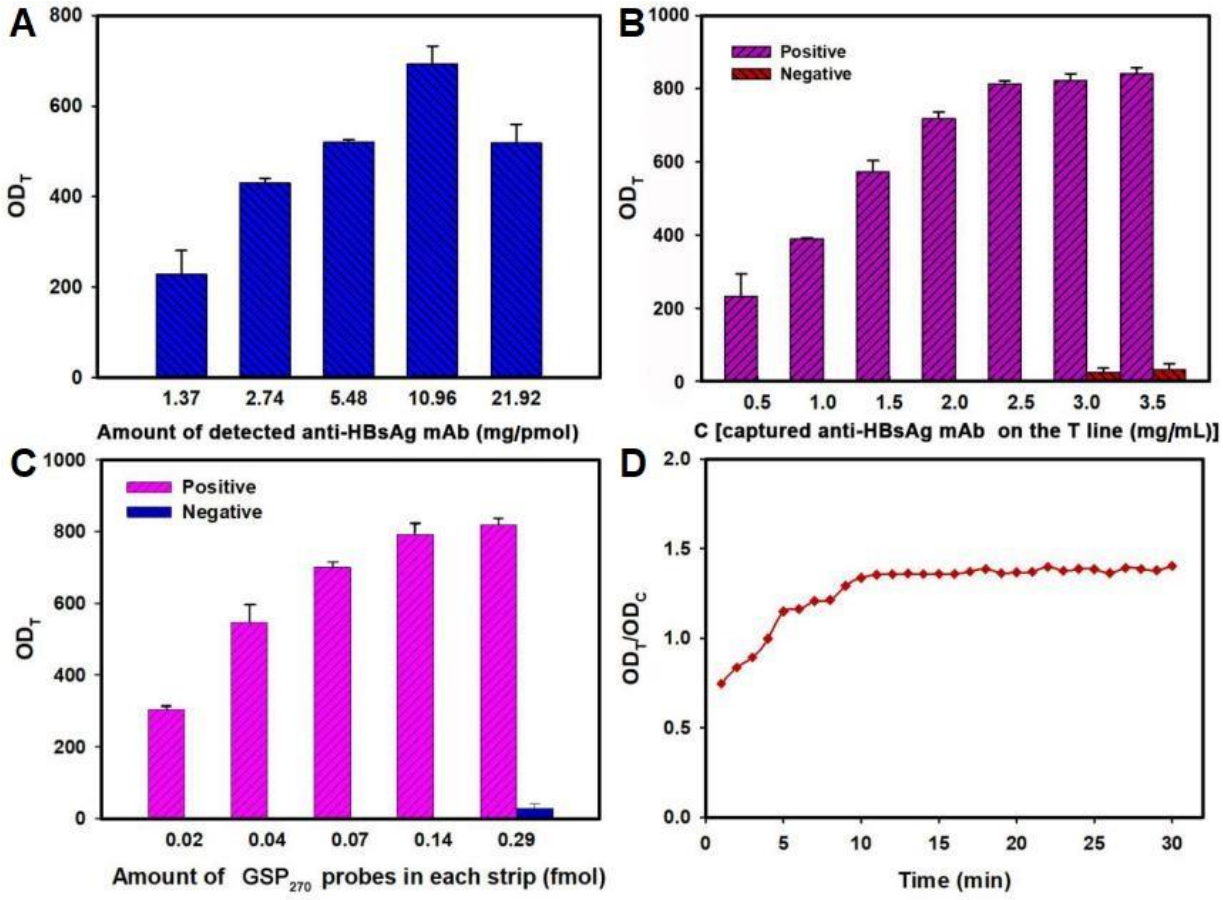

Figure S20. Parameter optimization of GSP_{270}-LFIA for HBsAg detection. (A) The saturated labeling amount of detected anti-HBsAg mAb on the GSP_{270} surface. (B) The concentration of captured anti-HBsAg mAb sprayed on the T line. (C) The used amount of GSP_{270} probe in each strip. (D) The optimal readout time after running the strip with the sample solution.

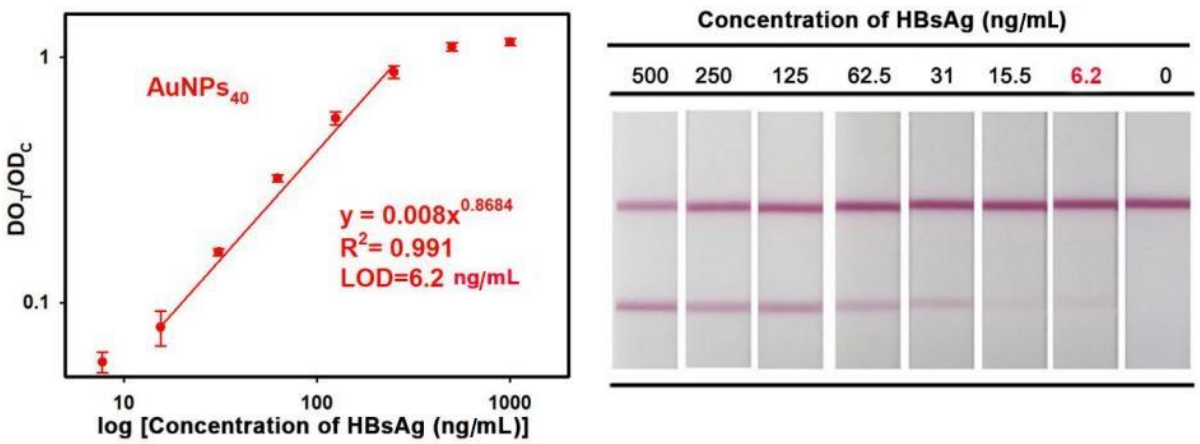

Figure S21. AuNP$_{40}$-LFIA strips for HBsAg detection in serum.

Table S1. Synthesis conditions of different GSPs.

Size (nm)	Oleylamine-coated AuNPs (mg)	PMAO (mg)	SDS (mg)	Oil/water (μL/μL)	Ultrasonic power (960 W)
100 nm	10	0.5	6	50/500	8%
160 nm	10	0.5	4	50/500	8%
200 nm	10	0.5	2.5	20/500	10%
270 nm	10	0.5	2.5	20/500	16%
400 nm	10	0.5	2.5	20/500	20%

Table S2. The optimal experimental condition combinations used for HCG detection with GSP-LFIA or AuNP-LFIA.

Labels	pH	The EDC concentration (μg/mL)	The saturated labeling amount of anti-HCG-β mAbs (mg/pmol)	Tapture mAbs sprayed on the T line (mg/mL)	The GSP or AuNP probe amount used in each strip (fmol)	The running time for signal readout (min)
$AuNP_{40}$	7	3.125	0.321	2.5	6.23	15
$AuNP_{80}$	7	3.125	0.625	2.5	1.28	15
$AuNP_{120}$	7	3.125	1.5625	2.5	0.64	15
$AuNP_{180}$	7	6.25	3.125	2.5	0.8	20
GSP_{100}	7	3.125	5	2.5	3.2	15
GSP_{160}	7	3.125	5	2.5	1.2	15
GSP_{200}	7	3.125	10	2.5	0.496	15
GSP_{270}	7	3.125	12	2.5	0.216	15
GSP_{400}	7	3.125	10	2.5	0.104	15

Table S3. Correlation analysis for HBsAg detection in serum among three methods, including GSP_{270}-LFIA, $AuNP_{40}$-LFIA, and the clinically well-accepted CLIA kits.

Sample	GSP_{270}-LFIA		$AuNP_{40}$-LFIA		CLIA
	Detected concentration (ng/mL)	CV (%)	Detected concentration (ng/mL)	CV (%)	Detected concentration (ng/mL)
1	133.82 ±7.35	5.49	111±22.8	20.54	156.6
2	120.45 ±4.17	3.46	141±15.66	11.10	147.3
3	88.87±1.90	2.13	80±14.24	17.8	99.2
4	83.09 ±5.64	6.79	90.6±6.51	7.18	102.3
5	62.34 ±2.47	3.96	42.5±13.44	31.62	78.4
6	57.90 ±6.59	11.38	75±24.24	32.32	60.5
7	114.28 ±1.92	3.35	106.05±14.21	13.39	121.08
8	48.62 ±1.89	3.89	33.23±9.53	28.67	58.3
9	38.43 ±3.17	8.26	36.5±4.95	13.56	51.2
10	25.51 ±1.21	4.75	23.15±20.11	86.87	30.25
11	208.4 ±19.7	9.45	197.34±6.25	3.17	219
12	200.2 ±13.7	6.83	254.35±23.64	9.297	224
13	18.37 ±1.75	9.53	19.45±14.61	75.11	23.4
14	18.09 ±1.40	7.75	12.35±4.74	38.38	25.0
15	17.53 ±0.79	4.53	16.5±1.78	10.78	20.0
16	15.29 ±0.87	5.71	23.75±1.20	5.05	16.3
17	153±0.61	4.02	149.42±3.65	2.44	163.3
18	12.55 ±0.98	7.80	9.7±0.67	6.91	18.32
19	7.54 ±1.01	13.41	13.2±1.18	8.94	10.0
20	6.32 ±0.82	13.06	9.55±0.16	1.68	8.0
21	66.25 ±8.77	13.23	64.34±8.24	12.81	75
22	86.02 ±7.01	8.15	67.35±5.34	7.93	100
23	4.90±0.22	4.49	ND		5.0
24	78.61±0.67	14.44	68.33±9.43	13.81	75.3
25	3.45 ±1.08	31.37	6.53±1.23	18.86	6.0
26	3.13 ±0.19	6.07	ND		4.5
27	2.74 ±0.20	7.44	ND		4.0
28	30.02±0.42	20.57	39.63±5.77	14.56	45.5
29	2.02 ±0.08	3.88	ND		3.0
30	1.76 ±0.14	7.95	ND		2.6
31	1.49 ±0.21	14.06	ND		2.0
32	1.25 ±0.33	26.73	ND		1.5
33	0.88 ±0.09	10.22	ND		1.0
34	0.44 ±0.14	30.96	ND		0.8
35	0.41 ±0.09	22.68	ND		0.5
36	ND		ND		ND
37	ND		ND		ND
38	ND		ND		ND
39	ND		ND		ND
40	ND		ND		ND
41	ND		ND		ND
42	ND		ND		ND
43	ND		ND		ND
44	ND		ND		ND
45	ND		ND		ND

Table S4 A comparison of the detection performance of our GSPs based LFIA and other reported gold-based immunoassay methods.

Method	Signal output mechanism	Linear range	Limit of detection	Reference
GSPs based LFIA	GSPs	0.46 ~1000 ng/mL	0.46 ng/mL	This work
Capacitive immunosensor[1]	Planar gold nanoparticles	10 ~ 60 ng/mL	10 ng/mL	Anal. Methods 2013, 5, 4448
Homogeneous fluorescence assay[2]	Europium-chelate-adsorbed silica nanoparticles	10 ~ 200 ng/mL	10 ng/mL	Anal. Methods 2012,4, 3810–3815.
Enhanced LFIA[3]	Dual gold nanoparticle conjugates	0.1 ~ 30 ng/mL	0.06 ng/mL	ACS Omega 2019, 4, 5083-5087
Electrochemical immunoassay[4]	Antigen-antibody reaction combined with nanogold	0.5 ~ 650 ng/mL	0.1 ng/mL	Microchim. Acta. 2009, 166, 269–275.
Conductometric immunoassay[5]	Double-codified nanogold particles	0.1 ~ 600 ng/mL	0.01 ng/mL	Biochem. Eng. J. 2009, 45, 107–112.
Dynamic light scattering[6]	Target-induced aggregation of gold nanoparticles	0.0051 IU/mL	0.005 IU/mL	Anal. Biochem 2012, 428, 119–125
Surface-enhanced Raman scattering (SERS)[7]	Gold nanoflower based SERS	0.03 ~ 0.62 IU/mL	0.01 IU/mL	Biosens. Bioelectron. 2015,66, 461–467
Localized surface plasmon resonance (LSPR)[8]	Gold nanorod based LSPR	0.01 ~ 1 IU/mL	0.01 IU/mL	Biosens. Bioelectron. 2010, 26, 404–410

Calculation of extinction Molar decadic extinction coefficient ε

ε of AuNPs and GSPs were calculated according to the Lambert-Beer[9]:

$$\varepsilon = \frac{A}{CL} \quad (1)$$

where A is the UV–vis absorbance of the nanoparticle solution, and L is the path length of the measuring beam in the sample. C is the concentration of the nanoparticles. AuNPs with a size of 80nm, 120nm and 180 were synthesized following a kinetically controlled seeded growth strategy. Hence, C_{AuNPs} was obtained from the concentration of seed gold, which was calculated according to a previous research.[10]

Furthermore, the C_{GSPs} were calculated form the following formula:

$$C = \frac{(m_1\rho_2 + m_2\rho_1)\ P}{\frac{4}{3}\prod R^3\rho_1\rho_2 NAXV} \quad (2)$$

Where m_1 and m_2 is the adding quality of the oleylamine-coated AuNPs and the PMAO when synthesizing different sized of GSPs, respectively. The ρ_1 and ρ_2 are the densities of the Au and the PMAO, respectively. The R refers to the radius of GSPs, and V is the volume of the sample solution, NA is the Avogadro's number. P is the productive rate of GSPs, and where x is the dilution ratio of the measuring sample.

Calculation of the number of internal oleylamine-coated AuNPs in each different sized GSP

The number (N) of internal oleylamine-coated AuNPs in each different sized GSPs were estimated according to the following formula:

$$N = \frac{\rho_2 \mathrm{m}_1 R_x^{\ 3}}{(m_1\rho_2 + m_2 p_1) P R_0^{\ 3}} \quad (3)$$

Where Rx and R_0 is the radius of GSPs and the oleylamine-coated AuNPs, respectively.

References

1. Alipour E, Ghourchian H, Boutorabi S M. Gold nanoparticle based capacitive immunosensor for detection of hepatitis B surface antigen. Anal Methods. 2013; 5 (17):4448-53.
2. Dou XR, Wu ZZ, Hu ZY, Zhu XT, Xu R, Xie L, et al. Preparation of immuno-probes based on europium-chelate-adsorbed silica nanoparticles and magnetic nanoparticles and their application in detection of hepatitis B surface antigen. Anal Methods. 2012; 4: 3810-5.
3. Shen Y, Shen G. Signal-enhanced lateral flow immunoassay with dual gold nanoparticle conjugates for the detection of hepatitis B surface antigen. ACS Omega. 2019; 4: 5083-7.
4. Wu S, Zhong Z, Wang D, Li M, Qing Y, Dai N, et al. Gold nanoparticle-labeled detection antibodies for use in an enhanced electrochemical immunoassay of hepatitis B surface antigen in human serum. Microchim Acta. 2009; 166: 269-75.
5. Liu H, Yang Y, Chen P, Zhong Z. Enhanced conductometric immunoassay for hepatitis B surface antigen using double-codified nanogold particles as labels. Biochem Eng J. 2009: 45: 107-112.
6. Wang X, Li Y, Quan D, Wang J, Zhang Y, Du J, Peng J, Fu Q, Zhou Y, Jia S. Detection of hepatitis B surface antigen by target-induced aggregation monitored by dynamic light scattering. Anal. Biochem. 2012; 428: 119-25.
7. Kamińska A, Witkowska E, Winkler K, Dzięcielewski I, Weyher J L, Waluk J. Detection of Hepatitis B virus antigen from human blood: SERS immunoassay in a microfluidic system. Biosens Bioelectron. 2015; 66: 461-7.
8. Wang X, Li Y, Wang H, Fu Q, Peng J, Wang Y, Du J, Zhou Y, Zhan L. Gold nanorod-based localized surface plasmon resonance biosensor for sensitive detection of hepatitis B virus in buffer, blood serum and plasma. Biosens Bioelectron. 2010; 26: 404-10.
9. Mäntele W, Deniz E, UV–vis absorption spectroscopy: lambert-beer reloaded. Spectrochim. Acta Part A. 2017;173: 965-8.
10. Haiss W,Thanh NT, Aveyard J, Fernig DG, Determination of size and concentration of gold nanoparticles from UV-vis spectra. Anal Chem. 2007; 79: 4215-21.